IEEE Photonics Journal
An IEEE Photonics Society Publication

All-Fiber Tunable LP_{11} Mode Rotator With 360° Range

Volume 8, Number 5, October 2016

Zhikun Hong
Songnian Fu
Dawei Yu
Ming Tang, ***Senior Member, IEEE***
Deming Liu

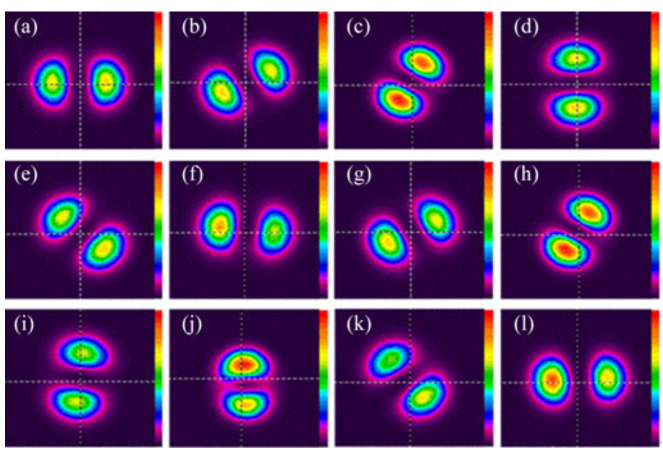

DOI: 10.1109/JPHOT.2016.2605822
1943-0655 © 2016 IEEE

All-Fiber Tunable LP_{11} Mode Rotator With 360° Range

Zhikun Hong, Songnian Fu, Dawei Yu, Ming Tang, *Senior Member, IEEE*, and Deming Liu

National Engineering Laboratory for Next Generation Internet Access System, School of Optics and Electronic Information, Huazhong University of Science and Technology, Wuhan 430074, China

DOI:10.1109/JPHOT.2016.2605822

Manuscript received June 22, 2016; revised August 28, 2016; accepted August 31, 2016. Date of publication September 2, 2016; date of current version September 19, 2016. This work was supported by the National Natural Science Foundation of China under Grant 61575071 and Grant 61331010 and in part by the ZTE Industry-Academia-Research Cooperation Funds. Corresponding author: S. Fu (e-mail: songnian@mail.hust.edu.cn).

Abstract: We propose and experimentally demonstrate an all-fiber tunable LP_{11} mode rotator with 360° range, based on the bending and twisting of the two-mode fiber (TMF). A theoretical model of TMF perturbation and its effect on the spatial pattern of LP_{11} mode is put forward. We experimentally characterize the implementation of the LP_{11} mode rotator by an all-fiber polarization controller configuration. The results agree well with the theoretical investigations. We are able to demonstrate arbitrary LP_{11} mode rotation with 360° range. The insertion loss is less than 0.4 dB when the operation wavelength is varied from 1540 to 1560 nm.

Index Terms: Few-mode fiber, liquid crystal on silicon (LCOS), mode division multiplexing (MDM), mode rotation.

1. Introduction

Recently, the mode division multiplexing (MDM) technique based on few-mode fiber (FMF), together with multi-input multi-output (MIMO) signal processing, has captured worldwide research interest due to its potential to solve future capacity crunch arising in single mode fibers (SMF) [1], [2]. The most popular mode basis used in the current MDM transmission is linearly polarized (LP) modes, which are the linear combination of corresponding vector modes of the FMF. Generally, LP modes in the FMF can be divided into two types according to their spatial symmetry characteristics, i.e., the circular symmetric modes and non-circular symmetric modes [3]. Taking the LP_{0m} mode as an example, the electric field distribution along the angular direction is continuous and the amplitude is the same under the same radius. Thus, it can be called circular symmetric mode. Whereas the LP_{lm} ($l \geq 1$) mode is non-circular symmetric mode, because the electric field distribution along the angular direction is divided into several segmentations. Mode division multiplexers/de-multiplexers (MMUX/DeMMUX), which can combine/separate individual LP modes, are critical devices for the MDM implementation [4], [5]. However, there occurs one designated mode orientation for non-circular symmetric modes [5]. Only when the LP mode has the same orientation as required by the DeMMUX, can the mode division de-multiplexing be successfully implemented with low mode crosstalk. Otherwise, mode division de-multiplexing may end up with complex MIMO signal processing. Moreover, for a passive optical network based on the MDM technique [6], it is highly desired to align the orientation of LP_{11} mode with that of the designed phase plate for correct mode conversion with low cost. Ideally, the orientation of LP_{11} mode evolves periodically between LP_{11a} and LP_{11b} as it propagates along the FMF [7]. However, the induced perturbation will destroy such perfect propagation in practical situations. Mode rotation of LP_{11} mode means that the mode pattern keeps its two-lobe intensity profile, but the line through two maximum power points of two lobes rotates. Until now, only LP_{11} mode rotator based on specially designed planar lightwave circuit (PLC) technique has been reported [8]. Mode orientation rotation is achieved with an insertion loss (IL) of less than 0.46 dB from LP_{11a} to LP_{11b} over the wavelength range from 1450 nm to 1650 nm. However, the IL is increased due to the fiber coupling issue. All-fiber devices, such as fiber tapering based photonic lantern, are attractive solutions [9], due to their advantages including low IL, compact package, and wideband operation. Therefore, theoretical investigation of LP_{11} mode rotation by polarization maintaining few mode fiber has also been proposed [10]. However, the rotation angle of spatial orientation is fixed once the length of polarization maintaining few mode fiber is fixed.

In this paper, we theoretically investigate the birefringence arising in two-mode fiber (TMF) by the form of Jones matrix and identify two variations of LP_{11} mode profile. One is the mode rotation and the other one is the mode distortion along angular direction. When the TMF is properly perturbed, pure mode rotation without mode distortion can be realized. Finally, we are able to demonstrate an all-fiber LP_{11} mode rotator with less than 0.4 dB IL over 360° range, by a TMF-based conventional polarization controller (PC) configuration.

2. Theoretical Analysis

For current MDM transmission, LP pseudo-mode basis is commonly used because LP modes are more readily excited and detected than the true vector modes. LP modes can be treated as a linear combinations of true vector modes [11], [12]. Specifically, the LP_{11} mode is a linear combination of four vector modes including TM_{01}, TE_{01}, HE_{21a}, and HE_{21b}, which can be defined as an LP_{11} mode cluster [13]. Here, we take the rotation of LP_{11ax} mode as an example, which is composed of TM_{01} and HE_{21a} modes with mathematical expressions given by [14]

$$e_{\mathrm{TM01}} = F(r)\begin{bmatrix}\cos\phi\\ \sin\phi\end{bmatrix} \tag{1}$$

$$e_{\mathrm{HE21a}} = F(r)\begin{bmatrix}\cos\phi\\ -\sin\phi\end{bmatrix} \tag{2}$$

where $F(r)$ is a radial function, and ϕ is the angle with respect to the x-axis. The mathematical expression of input LP_{11ax} mode is

$$e_{\mathrm{LP11ax}} = e_{\mathrm{TM01}} + e_{\mathrm{HE21a}} = 2F(r)\cos\phi\begin{bmatrix}1\\ 0\end{bmatrix}. \tag{3}$$

The unit Jones vector $\hat{e}_0 = [\,1\ 0\,]^{\mathrm{T}}$ means that the state of polarization (SOP) is fixed at horizontal linear polarization. When a section of TMF is perturbed, the rotation of mode LP_{11ax} at the output of the TMF can be described as (4), shown below, which is obtained by rotation of coordinate

$$e_{\mathrm{output\_LP11}\theta x} = 2F(r)\cos(\phi - \theta)\begin{bmatrix}\cos\theta\\ \sin\theta\end{bmatrix} \tag{4}$$

where θ is anticlockwise rotation angle. The unit Jones vector $\hat{e}_\theta = [\,\cos\theta\ \sin\theta\,]^{\mathrm{T}}$ indicates that the state of polarization is still along the line through two maximum power points of two lobes. For ease of calculation, radial distribution function $F(r)$ can be reasonably ignored in the following derivation. Then, the transmission matrix of a TMF section can be described by [15], [16]

$$e_{\mathrm{output\_LP11}\theta x} = J_{\mathrm{TM01}}e_{\mathrm{TM01}} + J_{\mathrm{HE21a}}e_{\mathrm{HE21a}} \tag{5}$$

$$e_{\mathrm{output\_LP11}\theta x} = J_{\mathrm{TM01}}\begin{pmatrix}\cos\phi\\ \sin\phi\end{pmatrix} + J_{\mathrm{HE21a}}\begin{pmatrix}\cos\phi\\ -\sin\phi\end{pmatrix} \tag{6}$$

where J_{TM01} and J_{HE21a} are corresponding Jones matrices for vector modes TM_{01} and HE_{21a}, respectively. Under the condition of $\theta = 0$, the output of all-fiber mode rotator is still mode LP_{11ax}. The corresponding Jones matrices are

$$J^0_{\mathrm{TM01}} = J^0_{\mathrm{HE21a}} = \begin{pmatrix}1 & 0\\ 0 & 1\end{pmatrix}, \tag{7}$$

Next, for an arbitrary rotation angle θ, we can work out

$$J^\theta_{\mathrm{TM01}} = \begin{pmatrix}1 & 0\\ 0 & 1\end{pmatrix} \tag{8}$$

$$J^\theta_{\mathrm{HE21a}} = \begin{pmatrix}\cos 2\theta e^{j2n\pi} & -\sin 2\theta e^{j2n\pi}\\ \sin 2\theta e^{j2n\pi} & \cos 2\theta e^{j2n\pi}\end{pmatrix}, \tag{9}$$

For the unperturbed TMF, propagation constants of individual vector modes of TE_{01}, TM_{01}, and HE_{21} are slightly different [17]. Thus, modal birefringence occurs [18]. Consequently, for the unperturbed TMF, Jones matrix of TM_{01} and HE_{21a} are unit matrices except for different phase shift, leading to a periodical spatial pattern variation between LP_{11a} and LP_{11b} mode. However, the situation is different for the perturbed TMF. Effective refractive index (RI) of individual vector modes may have different modifications. As shown in (8), Jones matrix for TM_{01} mode is a unit matrix, in order to realize given angle rotation. Thus, such section of perturbed TMF can be treated as a waveplate for TM_{01} mode. However, (9) indicates that the SOP of HE_{21a} mode rotates under the same perturbation induced birefringence. Generally, (8) and (9) cannot be simultaneously satisfied after the TMF perturbation. In those conditions, mode distortion happens and distorted intensity profile are observed by numerical calculation, as shown in Fig. 2(e)–(h). In order to further verify our theoretical analysis, we consider two special scenarios. First, we discuss the contribution of modal birefringence without birefringence of involved vector modes. In such case, perturbation is not induced and spatial pattern of LP_{11} mode only varies between LP_{11a} and LP_{11b} mode [7]. Thus, arbitrary mode rotation will not happen. Second, we discuss the contribution of birefringence of involved vector modes without modal birefringence. In such case, effective RIs of TM_{01} and HE_{21a} are theoretically set to the same value. Therefore, LP_{11ax} will keep its two-lobe intensity, when the TMF is not perturbed. When perturbation such as bending or twisting happens, we can solve the problem of light propagation as classical anisotropic medium optics with two principal axes [19]. As a result, when LP_{11ax} mode propagates along the TMF entwined with the PC configuration, SOP of the two-lobe pattern can be various, but the mode profile keeps unchanged all the time. By only taking into account of birefringence of involved vector modes without modal birefringence, neither mode rotation nor distortion occurs.

3. System Configuration and Characterization Results

Next, we experimentally investigate the proposed all-fiber LP_{11} mode rotator, as shown in Fig. 1. The optical source is a tunable distributed feedback (DFB) laser diode (LD), while the operation wavelength is initially set at 1550 nm for the subsequent characterizations. The light is divided into two parts by a 1×2 optical coupler with a power ratio of 70:30. One beam with 70% power is coupled into a liquid crystal on silicon (LCOS) based mode selective convertor, and the other is reserved for further phase retardation characterization of the LP_{11} mode. After mode selective conversion, LP_{11ax} mode is launched into a section of step-index TMF (OFS) with 19-μm core diameter and a RI difference between core and cladding of 0.0034. Due to the effective RI difference of involved vector modes, spatial pattern of LP_{11} mode changes periodically between LP_{11a} and LP_{11b} modes [7]. And the spatial periodicities of two different LP_{11} modes in this TMF are $Z_{\mathrm{TE-HE}}$ = 0.55 m and

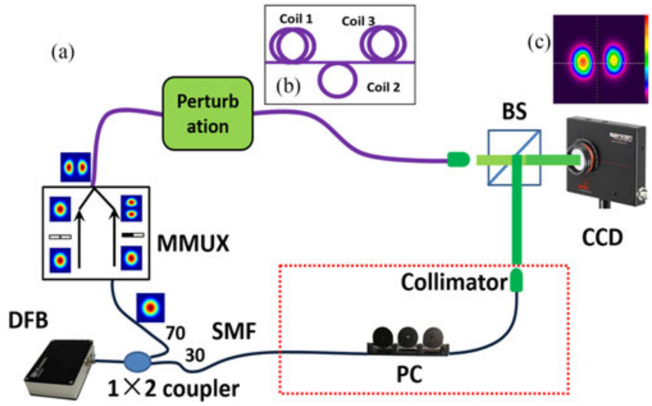

Fig. 1. (a) Experimental setup. (b) PC configuration of LP_{11} mode rotator. (c) Initial LP_{11ax} mode.

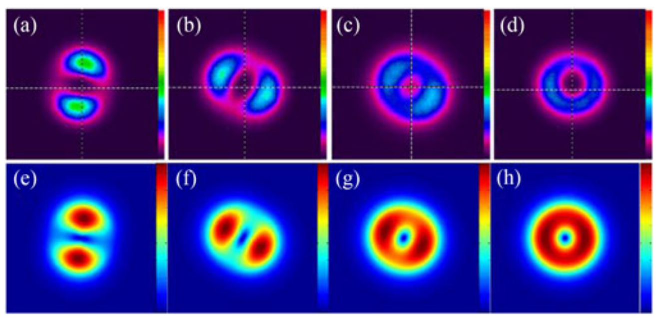

Fig. 2. (a)–(d) show the captured LP_{11} mode spatial pattern under various manual perturbations. (e)–(h) show the calculated results based on (6), when two Jones matrices do not satisfy (8) and (9) simultaneously.

$Z_{\mathrm{TM-HE}} = 2.70$ m, respectively [20]. After transmission through 3-m-long TMF, the output light is collimated and then passed through a beam splitter (BS). An infrared CCD camera is used to capture the mode field distribution. For the ease of comparison, the input spatial pattern of LP_{11ax} mode is shown in Fig. 1(c).

The TMF is manually twisted for the purposed of perturbation, and the output mode field deviates from the ideal LP_{11a} mode spatial pattern, as shown in Fig. 2(a)–(d). The power spreads along the annulus, instead of two discrete lobes. Both the rotation and mode distortion of the LP_{11ax} mode can be observed. Meanwhile, the numerically calculated results are also shown in Fig. 2(e)–(h). Noticeably, Jones matrices leading to mode distortion are not unique, compared with pure mode rotation. But we are confident about the existence of corresponding Jones matrices leading to pure mode rotation from the experiment. In particular, no matter how the stress induced birefringence changes, the power almost keeps off the center of the captured field, indicating that no mode coupling between LP_{01} mode and LP_{11} mode is observed.

Although the Jones matrices for pure mode rotation can be analytically determined, as shown in (8) and (9), practical implementations are various. In order to realize fine perturbation in a convenient way, instead of manually twisting the TMF, we entwine the TMF into commercial PC whose paddle size is 32 mm. We combine three paddles one by one like traditional single mode fiber-based PC. By adjusting three paddles, we are able to realize the LP_{11} mode orientation rotation within 360° range. During our experiment, we try several combinations of coil numbers under condition of the paddle size of 32 mm, such as (1, 1, 1), (1, 2, 1), (1, 1, 2), (2, 0, 2), (2, 1, 2), and (2, 2, 2). Full mode rotation can only be achieved by (2, 1, 2) and (2, 2, 2). When the coil number is further decreased, full range mode rotation is impossible. The more coil number of each paddle is implemented, the easier we can observe full range pure rotation of LP_{11} mode. However, less

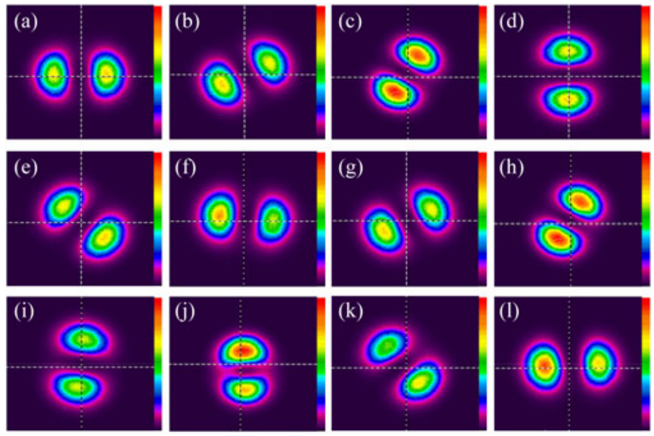

Fig. 3. Captured LP_{11} mode orientation rotation. (a) 0°, (b) 30°, (c) 60°, (d) 90°, (e) 135°, (f) 175°, (g) 210°, (h) 255°, (i) 265°, (j) 270°, (k)315°, and (l) 360°.

TMF consumption is always desired. Thus, we finally set three paddles with coil number (2, 1, 2). We also examine other PC with different paddle size, and pure mode rotation can still be achieved with different coil numbers. The captured LP_{11} mode field distribution with different orientation angles are summarized in Fig. 3(a–l). The LP_{11} mode with arbitrarily designated orientation angle can be achieved with fine adjustment of the PC configuration and we only show some examples here. We notice that the captured two lobes of LP_{11} mode have different intensity. We infer two sources may be responsible for this phenomenon. One is the residual LP_{01} mode with extremely low power, resulting in different intensity of two lobes. Another reason is the cleanliness of the fiber output end. When the fiber is not cleaned, severe distortion will be observed by the captured mode pattern. Next, the rotating efficiency can be determined by calculating the correlation coefficient between experimentally rotated LP_{11} mode and theoretically calculated standard LP_{11} mode at the designated orientation

$$\eta = \frac{\left|\iint_S u_1(x, y) \cdot u_2(x, y)^* dxdy\right|^2}{\iint_S |u_1(x, y)|^2 dxdy \iint_S |u_2(x, y)|^2 dxdy} \tag{10}$$

where $u_1(x, y)$ is the captured LP_{11} mode, $u_2(x, y)$ is the calculated standard LP_{11} mode after orientation rotation, and * represents complex conjugate. As a result, the calculated rotating efficiency of all rotated LP_{11} modes are higher than 0.884. During the characterization, we are also curious about the SOP of the rotated LP_{11} mode. With the aid of polarizer, SOP of rotated LP_{11} mode is determined. Fig. 4(a)–(d) show the intensity pattern of LP_{11} mode after the operation of pure mode rotation with different angles. Then, the maximum intensity profile can be observed, as shown in Fig. 4(e)–(h), when the polarizer is aligned with the line through two points of maximum electric amplitude between two lobes. When we adjust the polarizer to its orthogonal direction, the mode patterns disappear, as shown in Fig. 4(i)–(l). Since the extinction ratio of polarizer is more than 20 dB, we can conclude that the rotated LP_{11} mode is still linearly polarized and its SOP also rotates the same value as that of spatial pattern rotation. As a result, (4) is successfully verified.

Next, we find that the mode field distributions in Fig. 3(b) and (g) are almost the same. However, actually, Fig. 3(g) is captured after 180° orientation angle rotation. Therefore, it is necessary to identify the rotation of 180°. Since the LP_{11} mode naturally has π phase retardation between the two lobes, we can distinguish two fields by the method of optical interference. After collimation, the reserved light from another output port of the 1 × 2 coupler with 30% power is combined with LP_{11} mode through the BS. The linewidth of used DFB laser is less than 1 MHz, leading to a coherent length of more than 300 m. Since optical path difference between LP_{11} mode and LP_{01} mode is almost the same by optimizing the length of single mode fiber, we can manage the phase difference

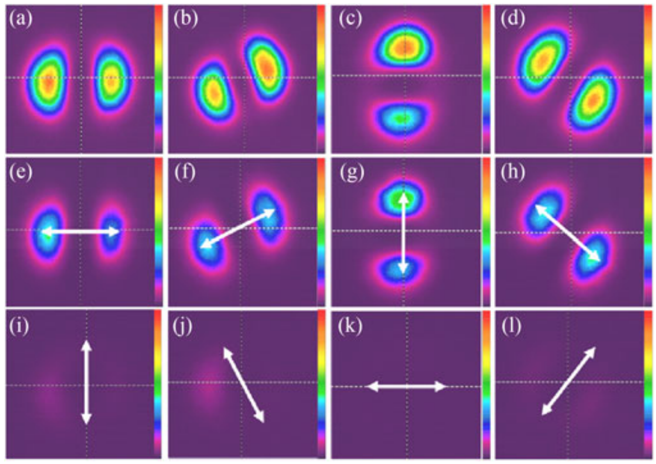

Fig. 4. Captured LP_{11} mode with different orientation rotation with polarization resolved measurement. The arrows indicate the direction of the polarizer's axis.

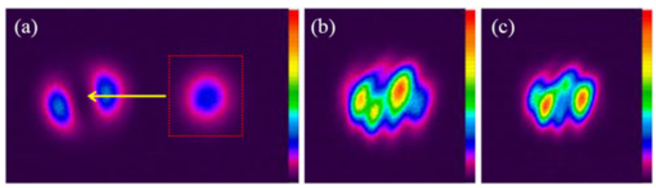

Fig. 5. (a) Mode profile before moving the fundamental mode spot to overlap with the LP_{11} model field. (b) and (c) are the captured interference patterns before and after a 180° rotation of mode orientation.

between LP_{01} mode and one lobe of LP_{11} mode to be zero. Thus, there will be a constructive interference in this lobe and destructive interference occurs for the other lobe. If the orientation of LP_{11} mode is successfully rotated with 180º, the two lobes will change positions and consequently the interference patterns exchange the position. We are able to control the position of the collimated fundamental mode spot through a three-dimensional translation stage. When the output LP_{11} mode filed has the profile as shown in Fig. 3(b), we move the collimated spot of the reserved light to overlap with the LP_{11} mode field, as shown in Fig. 5(a). Strong interference, as shown in Fig. 5(b), can be observed. We record the position of the collimated reserved light spot, and then move it away. By tuning the mode rotator, we achieve the output field as shown in Fig. 3(g). Again, we move the fundamental mode spot back to the previous overlap position. The interference pattern changes to the pattern of Fig. 5(c). The region of constructive interference occurrence in Fig. 5(b) becomes destructive interference in Fig. 5(c), while the region of destructive interference in Fig. 5(b) becomes constructive interference in Fig. 5(c). Obviously, π phase retardation exists between two LP_{11} lobes. It is verified that the LP_{11} mode is indeed rotated by 180°. Finally, we characterize the IL of the proposed LP_{11} mode orientation rotator. We monitor the optical power when the LP_{11} mode is rotated with different orientation angles. The IL compared to the situation without mode rotation is summarized in Fig. 6. The IL induced by the mode orientation rotator is less than 0.4 dB, when the operation wavelength varies from 1540 nm to 1560 nm. Generally, the operation bandwidth limitation of proposed all-fiber mode rotator mainly comes from the operation wavelength of used TMF. We believe that pure mode rotation is expected to be achieved over the C-band. Thus, the proposed configuration can be used in practical MDM transmission with acceptable IL. Meanwhile, although the temperature may slightly change the mode effective index of involved vector modes, pure mode rotation can still be realized by finely adjusting the PC configuration with respect to environmental fluctuations.

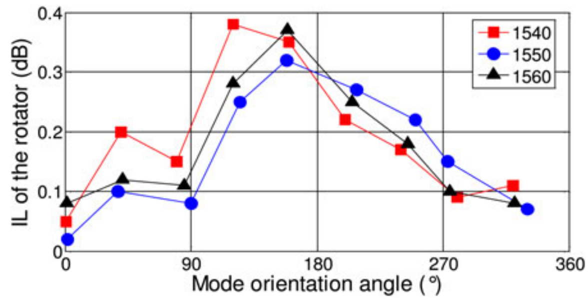

Fig. 6. IL of LP_{11} mode rotator with 360° range.

4. Conclusion

To the best of our knowledge, it is the first time that an all-fiber tunable LP_{11} mode rotator with 360° range is experimentally demonstrated. We have theoretically investigated the birefringence arising in the TMF by the form of Jones matrix. We find that mode rotation is possible due to the co-existence of birefringence of the involved vector modes and modal birefringence of the TMF. The experimental characterization under the condition of manually twisted TMF agrees well with the theoretical calculation. The insertion loss of proposed all-fiber LP_{11} mode rotator is less than 0.4 dB, when the operation wavelength is varied from 1540 nm to 1560 nm.

References

[1] R. Ryf *et al.*, "Mode-division multiplexing over 96 km of few-mode fiber using coherent 6 × 6 MIMO processing," *J. Lightw. Technol.*, vol. 30, no. 4, pp. 521–531, Feb. 2012.
[2] R. G. H. van Uden *et al.*, "Ultra-high-density spatial division multiplexing with a few-mode multicore fibre," *Nat. Photonics*, vol. 8, no. 11, pp. 865–870, Nov. 2014.
[3] D. Gloge, "Weakly guiding fibers," *Appl. Opt.*, vol. 10, no. 10, pp. 2252–2258, Oct. 1971.
[4] A. Li, X. Chen, A. A. Amin, and W. Shieh, "Fused fiber mode couplers for few-mode transmission," *Photon. Technol. Lett.*, vol. 24, no. 21, pp. 1953–1956, Nov. 2012.
[5] J. Xu, C. Peucheret, J. K. Lyngsø, and L. Leick, "Two-mode multiplexing at 2 × 10.7 Gbps over a 7-cell hollow-core photonic bandgap fiber," *Opt. Exp.*, vol. 20, no. 11, pp. 12449–12456, May 2012.
[6] T. Hu *et al.*, "Experimental demonstration of passive optical network based on mode-division-multiplexing," presented at the *Opt. Fiber Commun. Conf. Exhib.*, Paper Th2A.63.
[7] J. von Hoyningen-Huene, R. Ryf, and P. Winzer, "LCoS-based mode shaper for few-mode fiber," *Opt. Exp.*, vol. 21, no. 15, pp. 18097–18110, Jul. 2013.
[8] K. Saitoh *et al.*, "PLC-based LP11 mode rotator for mode-division multiplexing transmission," *Opt. Exp.*, vol. 22, no. 16, pp. 19117–19130, Jul. 2014.
[9] J. van Weerdenburg *et al.*, "10 Spatial mode transmission using low differential mode delay 6-LP fiber using all-fiber photonic lanterns," *Opt. Exp.*, vol. 23, no. 19, pp. 24759–24769, Sep. 2015.
[10] X. Zeng, Y. Li, W. Li, L. Zhang, and J. Wu, "All-fiber broadband degenerate mode rotator for mode-division multiplexing systems," *IEEE Photon. Technol. Lett.*, vol. 28, no. 13, pp. 1383–1386, Jul. 2016.
[11] D. J. Richardson, J. M. Fini, and L. E. Nelson, "Space-division multiplexing in optical fibres," *Nat. Photon.*, vol. 7, no. 5, pp. 354–362, May 2013.
[12] L. Palmieri and A. Galtarossa, "Coupling effects among degenerate modes in multimode optical fibers," *IEEE Photon. J.*, vol. 6, no. 6, pp. 1–8, Dec. 2014.
[13] S. Ramachandran, P. Kristensen, and M. F. Yan, "Generation and propagation of radially polarized beams in optical fibers," *Opt. Lett.*, vol. 34, no. 16, pp. 2525–2527, Aug. 2009.
[14] A. W. Snyder and J. D. Love, *Optical Waveguide Theory*, London, U.K.: Chapman and Hall, 1983.
[15] C. Kim, B. Choi, J. S. Nelson, Q. Li, P. Z. Dashti, and H. P. Lee, "Compensation of polarization-dependent loss in transmission fiber gratings by use of a Sagnac loop interferometer," *Opt. Lett.*, vol. 30, no. 1, pp. 20–22, Jan. 2005.
[16] C. Wu and H. Dong, "The general solution of noncircular uniform optical waveguides in an arbitrary coordinate system and its applications," *J. Lightw. Technol.*, vol. 20, no. 8, pp. 1604–1608, Aug. 2002.
[17] S. Ramachandran *et al.*, "Lifting polarization degeneracy of modes by fiber design: A platform for polarization-insensitive microbend fiber gratings," *Opt. Lett.*, vol. 30, no. 21., pp. 2864–2866, Nov. 2005.
[18] H. Kogelnik and P. J. Winzer, "Modal birefringence in weakly guiding fibers," *J. Lightw. Technol.*, vol. 30, no. 14, pp. 2240–2245, Jul. 2012.
[19] H. C. Lefevre, "Single-mode fibre fractional wave devices and polarization controllers," *Electron. Lett.*, vol. 16, no. 20, pp. 778–780, Sep. 1980.
[20] G. Volpe and D. Petrov, "Generation of cylindrical vector beams with few-mode fibers excited by Laguerre–Gaussian beams," *Opt. Commun.*, vol. 237, no. 1, pp. 89–95, Jul. 2004.